ARTICLE **OPEN**

Check for updates

Observation of information flow in the anti-$\mathcal{PT}$-symmetric system with nuclear spins

Jingwei Wen[1], Guoqing Qin[1], Chao Zheng[2], Shijie Wei[1,3], Xiangyu Kong[1], Tao Xin[4✉] and Guilu Long [1,3,5,6✉]

The recently theoretical and experimental researches on $\mathcal{PT}$-symmetric system have attracted unprecedented attention because of the various interesting features and potential applications in extending canonical quantum mechanics. However, as the counterpart of $\mathcal{PT}$-symmetry, there are few experimental researches on the anti-$\mathcal{PT}$-symmetric quantum system because of the challenges in simulating anti-$\mathcal{PT}$-symmetry in experiment. Here, we propose an algorithm for simulating the generalized anti-$\mathcal{PT}$-symmetric system in the quantum circuit model. Utilizing the algorithm, we demonstrated the quantum simulation of anti-$\mathcal{PT}$ system experimentally, and an oscillation of information flow is observed in a nuclear magnetic resonance quantum simulator. The experiment showed that the information could recover from the environment completely when the anti-$\mathcal{PT}$-symmetry is broken, whereas no information can be retrieved in the symmetry-unbroken phase. Our work opens the gate for the practical quantum simulation and experimental investigation of universal anti-$\mathcal{PT}$-symmetric system in a quantum computer.

npj Quantum Information (2020)6:28 ; https://doi.org/10.1038/s41534-020-0258-4

INTRODUCTION

The limitation on the Hermiticity of Hamiltonian can ensure the reality in the spectrum of energy eigenvalues and the unitarity of the resulting time evolution. However, a new class of non-hermitian Hamiltonian has attracted extensive attention and research because of the discovery by Bender and Boettcher in 1998[1]. It was found that Hamiltonians satisfying parity $\mathcal{P}$ (spatial reflection) and $\mathcal{T}$ (time reversal) symmetry instead of hermiticity can still have real energy spectra and orthogonal eigenstates in the symmetry-unbroken phase, in which the eigenfunction of system Hamiltonian is at the same time an eigenfunction of the joint $\mathcal{PT}$ operator[2,3]. When the Hamiltonian parameters cross the exceptional point, $\mathcal{PT}$-symmetry will be broken and lead to a symmetry-breaking transition[4]. This work has inspired numerous theoretical and experimental studies[5–17] of the non-hermitian systems, including demonstrating novel properties of quantum systems[14,15] and extending fundamental quantum mechanics[16,17].

Recently, another important counterpart anti-$\mathcal{PT}$-symmetry, which means the system Hamiltonian is anti-commutative with the joint $\mathcal{PT}$ operator $\{H, \mathcal{PT}\} = 0$, has attracted much research interest. Several interesting physical phenomena have been reported in the anti-$\mathcal{PT}$-symmetric systems, such as optical materials with balanced positive and negative index[18] and optical systems with constant refraction[19]. Some relevant experimental demonstrations have been realized in optical[18–23], atoms[24–26], electrical circuit resonators[27], and diffusive systems[28]. Quantum processes such as symmetry-breaking transition[24], simulation of anti-$\mathcal{PT}$-symmetric Lorentz dynamics[20], and observation of exceptional point[23,27] have been presented in these experiments, whereas the novel characteristics of entanglement[15,29,30] and information flow[13,31,32] in the anti-$\mathcal{PT}$-symmetric system, which would present various phenomena different from Hermitian quantum mechanics and reveal the relationship between system and environment, have not been fully and thoroughly investigated in the experiment.

In this work, we propose an algorithm for the simulation of generalized anti-$\mathcal{PT}$-symmetric evolution with a circuit-based quantum computing system using a three-qubit scheme and the simulation scheme is based on decomposing the non-Hermitian Hamiltonian evolution into a linear combination of unitary operators and realizing the simulation in an enlarged Hilbert space with ancillary qubits[33–35]. Compared with the generalized $\mathcal{PT}$-symmetric system, which can be simulated with one ancillary qubit[36], the simulation of generalized anti-$\mathcal{PT}$-symmetric system is more complicated, for instance, to simulate the two-level system, two ancillary qubits have to be used for the generalized anti-$\mathcal{PT}$-symmetric system. In particular, we found that information backflow in the $\mathcal{PT}$ system[13] is also present in the anti-$\mathcal{PT}$-system, and we have experimentally demonstrate the information flow oscillation for the first time on nuclear magnetic resonance quantum computing platform. We experimentally show that the information flow oscillates back and forth between the environments and system in broken phase and the phenomenon of information backflow occurs, which indicates information flows from the environment back to the system and this does not happen in traditional Hermitian quantum mechanics[37,38]. The oscillation period and amplitude increase as the system parameters approach the exceptional point. When passing through the critical point, the information backflow no longer occurs, and can only be attenuated exponentially from the system and leakage information into the environment. Moreover, in the time interval when the information backflow occurs, it indicates the presence of memory effects in the anti-$\mathcal{PT}$-symmetric system, which means the dynamics are non-Markovian[32,39]. Therefore, the phase-breaking and information flow transition at exceptional point observed in our experiment also mean the transition between non-Markovian process and Markovian process.

[1]State Key Laboratory of Low-Dimensional Quantum Physics and Department of Physics, Tsinghua University, 100084 Beijing, China. [2]Department of Physics, College of Science, North China University of Technology, 100144 Beijing, China. [3]Beijing Academy of Quantum Information Sciences, 100193 Beijing, China. [4]Shenzhen Institute for Quantum Science and Engineering, Southern University of Science and Technology, 518055 Shenzhen, China. [5]Frontier Science Center for Quantum Information, 100084 Beijing, China. [6]Beijing National Research Center for Information Science and Technology, 100084 Beijing, China. ✉email: xint@sustech.edu.cn; gllong@tsinghua.edu.cn
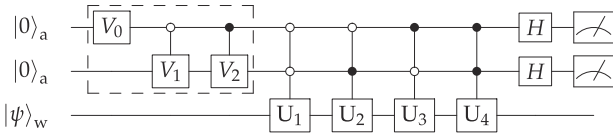
Fig. 1 Quantum circuits for the simulation of a generalized anti-$\mathcal{PT}$-symmetric single-qubit system. Single-qubit operators V_0 and H (Hardmard gate) are operated on the ancillary qubits and two two-qubit operators (0-controlled V_1 and 1-controlled V_2) are implemented to the system followed by four three-qubit controlled quantum gates $U_i (i \in [1, 2, 3, 4])$. At the end of the circuit, we measure the state vector of the work system in the subspace where the ancillary qubits are $|00\rangle\langle00|$.

RESULTS

Construction of simulation algorithm

We start from a more generalized form for a single-qubit anti-$\mathcal{PT}$-invariant Hamiltonian, which can be expressed as

$$\hat{H} = \begin{pmatrix} re^{i\theta} & is \\ i\mu & -re^{-i\theta} \end{pmatrix}, \tag{1}$$

where all the parameters r, θ, s, and μ are real numbers[16]. This generalized Hamiltonian will be the negative transpose of the original form under the action of joint operator $\mathcal{PT}$, where operator $\mathcal{P}$ is the Pauli σ_x matrix and $\mathcal{T}$ corresponds to complex conjugation. When the condition $s = \mu$ is satisfied as well, it can be reduced to the anti-commutation relation

$$(\mathcal{PT})\hat{H}(\mathcal{PT})^{-1} = -\hat{H}^T = -\hat{H}, \tag{2}$$

where notation A^T means the transpose of matrix A. The eigenvalues of Hamiltonian $\hat{H}$ are $\varepsilon_\pm = ir\sin\theta \pm \sqrt{r^2\cos^2\theta - \mu s}$ and the system is termed in the regime of unbroken anti-$\mathcal{PT}$-symmetric phase when $r^2\cos^2\theta - \mu s < 0$. For convenience, we set the difference between the two eigenvalues as $w = \varepsilon_+ - \varepsilon_- = 2\sqrt{r^2\cos^2\theta - \mu s}$. The dynamic evolution governed by the non-Hermitian Hamiltonian in Eq. (1) can be described by

$$\hat{\rho}(t) = \frac{e^{-i\hat{H}t}\hat{\rho}(0)e^{i\hat{H}^\dagger t}}{\text{tr}[e^{-i\hat{H}t}\hat{\rho}(0)e^{i\hat{H}^\dagger t}]}. \tag{3}$$

Here we employ the usual Hilbert–Schmidt inner product instead of a preferentially selected one and consider the effective non-unitary dynamic of an open quantum system[13,40]. Suppose that the non-unitary evolution operator U can be decomposed into the form $U = \sum_{i=1}^{d} a_i U_i$, where U_i are unitary oprators and coefficients a_i depend on the choice of decomposition but satisfy construction condition $\sum_{i=1}^{d} |a_i| = a$. Then, by constructing operators $\hat{G} = \sum_{i=1}^{d} \sqrt{\frac{a_i}{a}}|i\rangle\langle0|$ working on the ancillary qubits and controlled-operator $\hat{U} = \sum_{i=1}^{d}|i\rangle\langle i| \otimes U_i$, we can realize the simulation of Hamiltonian evolution in the subspace of $\langle 0|\hat{G}^\dagger\hat{U}\hat{G}|0\rangle$[34,41–43]. We construct a general quantum circuit to simulate the dynamic evolution in Eq. (3) by enlarging the system with ancillary qubits and encoding the subsystem with the non-Hermitian Hamiltonian with post-selection.

Quantum circuit used to simulate the generalized anti-$\mathcal{PT}$-symmetric evolution is shown in Fig. 1 including two ancillary qubits and one work qubit forming a three-qubit scheme. The initial state is prepared in $|00\rangle_a|\psi\rangle_w$ first, then an unitary operator V_0 and two two-qubit operators (0-controlled V_1 and 1-controlled V_2) are implemented on the ancillary qubits just as shown in the dotted box. The operation in the dotted box is equivalent to an operator V and only the first column is definable. The first column of two-qubit operator V without considering the normalization

constant is $[V_{11}, V_{21}, V_{31}, V_{41}]$ and

$$V_{11} = \cos(wt/2\hbar), \quad V_{21} = \frac{s+\mu}{w}\sin(wt/2\hbar),$$
$$V_{31} = i\frac{s-\mu}{w}\sin(wt/2\hbar), \quad V_{41} = \frac{-2ir\cos\theta}{w}\sin(wt/2\hbar), \tag{4}$$

It does not matter what the other matrix elements in operator V are, while we can determine the operator by Schmidt Orthogonalization under the constraint that the operator must be unitary. We can also decompose it into single and two-qubit operators just as shown in the dotted box of Fig. 1. Suppose that the normalized first column of the two-qubit operator is $[V'_{11}, V'_{21}, V'_{31}, V'_{41}]$ satisfying normalization conditions $\sum_{i=1}^{4}|V'_{i1}|^2 = 1$, and then we can construct 4×4 unitary matrix V that satisfies the constraint and the concrete form of operators can be determined by Eq. (5).

$$V = (V_1 \oplus V_2) \cdot (V_0 \otimes I), \tag{5}$$

where the single-qubit unitary operators V_0 and two-qubit controlled operators $V_k(k = 1, 2)$ can be formally expressed as rotation operators $R(\theta_l) = (\cos\theta_l \sin\theta_l \sin\theta_l - \cos\theta_l)$, $(l = 0, 1, 2)$. According to the deposition method and parameters in the generalized anti-$\mathcal{PT}$-symmetric Hamiltonian, we can determine the explicit forms of the angles in the three operators and the details are in the Methods. Next, the three-qubit controlled-U_i $(i = 1, 2, 3, 4)$ operators construct a set of complete basis in two-dimensional Hilbert space on the work system and the construction method is not unique, and the operators U_i can be simply set as identity matrix $\sigma_0 = I_{2\times2}$ and Pauli matrix $\sigma_x, \sigma_y, \sigma_z$. Finally, two Hardmard gates are applied on the ancillary qubits to mix up the states and the target quantum state $\hat{\rho}(t)$ of the work system can be obtained by measuring the work system in the subspace where the ancillary qubits are $|00\rangle\langle00|$ according to our parameters setup. It is worth emphasizing that our scheme works for both unbroken and broken anti-$\mathcal{PT}$-symmetric phase and even near the exceptional point, stability of the scheme is still very good. Therefore, our protocol provides a novel method to investigate various properties of anti-$\mathcal{PT}$-symmetric system and we apply it to the experimental observations of information flow.

Experimental implementation and results

To present the information retrieval in anti-$\mathcal{PT}$-symmetric system, we identify the information flow by trace distance to measure the distinguishability between two quantum states

$$D(\hat{\rho}_1(t), \hat{\rho}_2(t)) = \frac{1}{2}\text{tr}|\hat{\rho}_1(t) - \hat{\rho}_2(t)| \tag{6}$$

and $|\hat{M}| = \sqrt{\hat{M}^\dagger\hat{M}}$[31,32]. The trace distance keeps invariant under unitary transformations whereas does not increase under completely positive and trace-preserving maps, which means the unidirectional information flow from the system to environment will not be recovered. However, the complete information retrieval from the environment in $\mathcal{PT}$-symmetric system has been proposed in theory[13]. In contrast, there has been little research in the counterpart anti-$\mathcal{PT}$-symmetric system and in this work, we observed an oscillation of information flow in anti-$\mathcal{PT}$-symmetric single-qubit system in experiment based on our nuclear magnetic resonance platform.

As a proof-of-principle experiment, we consider a two-level anti-$\mathcal{PT}$-symmetric system

$$H_{APT} = s(i\hat{\sigma}_x + \lambda\hat{\sigma}_z), \tag{7}$$

where $s \geq 0$ is an energy scale and $\lambda \geq 0$ is a coefficient representing the degree of Hermiticity. We take different λ values in both anti-$\mathcal{PT}$-symmetric unbroken and broken region to observe the dynamic feature of the system. According to the definition of information flow, we need to evolve the system under anti-$\mathcal{PT}$-symmetric dynamics with different initial state $|0\rangle\langle0|$ and $|1\rangle\langle1|$ to determine the distinguishability. Hence, we
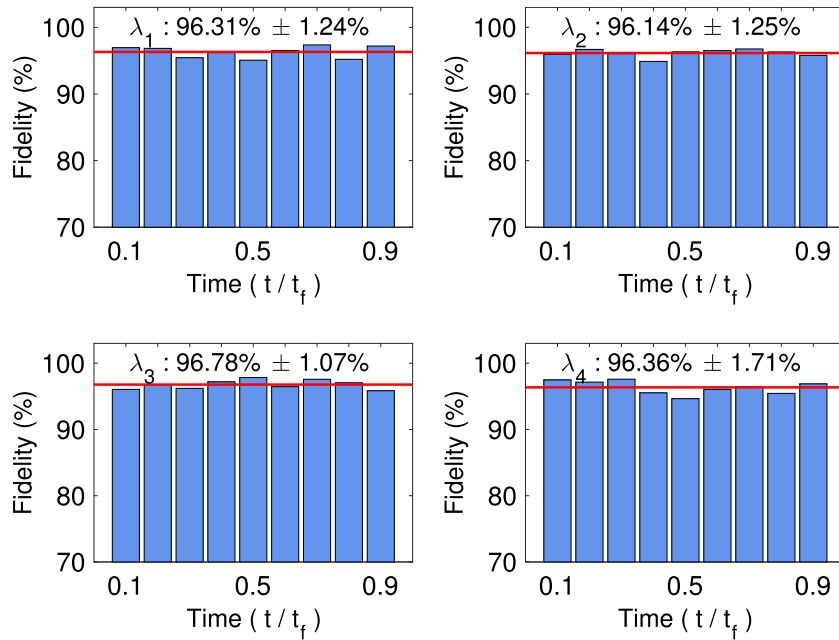
Fig. 2 Fidelities between the experimental results and theoretical expectation at nine discrete time points of different λ values. The average fidelities labeled by red lines are over 96% and the maximum deviations are within 2%.

add one more working system in experiment ensuring that the two working qubits undergo the same anti-$\mathcal{PT}$-symmetric evolution just with different initial states. We use the spatial averaging technique to prepare the pseudo-pure state[44,45] from the thermal equilibrium as the initial state and the form can be expressed as

$$|\rho_{0000}\rangle = (1 - \epsilon)I_{16}/2^4 + \epsilon|0000\rangle\langle0000|, \qquad (8)$$

where I_{16} is a 16×16 identity operator and $\epsilon \approx 10^{-5}$ is the polarization. The first item does not evolve under unitary operators and the second deviated part is equivalent to quantum pure state. The fidelities between experimental and ideal pure state $|0000\rangle$ are over 99.5%, which are calculated by the formula[46]

$$F(\rho, \sigma) = \text{tr}\,(\rho\sigma)/\sqrt{\text{tr}\rho^2}\sqrt{\text{tr}\,\sigma^2}. \qquad (9)$$

Subsequently, we apply the quantum operations in our algorithm according to the different parameter setup. Four values of $\lambda \in \{2, 1.5, 1.01, 0.5\}$ are chosen and the former three are located at broken phase and the last one leads to unbroken anti-$\mathcal{PT}$-symmetry. All the operations are realized using shaped pulses optimized by the gradient method [47]. Each shaped pulse is simulated to be over 99.5% fidelity while being robust to the static field distributions and inhomogeneity. By performing four-qubit quantum state tomography [48–50], we obtain the target density matrix when the ancillary qubits are $|00\rangle$ at the end of circuit. We extract experimental data at nine discrete time points and the mean fidelities between the theoretical expectations and experimental values are over 96% in Fig. 2. The information flow identified by experimental results are plotted in Fig. 3. Because of the random fluctuations of the amplitude and phase in control field, the experimental results produce some random errors. We suppose that the random fluctuations are within a range of 5% in amplitude and in phase, which are common in actual experimental process[51,52], then the fluctuation range of distinguishability are also plotted as the error bar.

DISCUSSION
Our experimental results clearly show that the distinguishability oscillates with evolution time when the system symmetry is
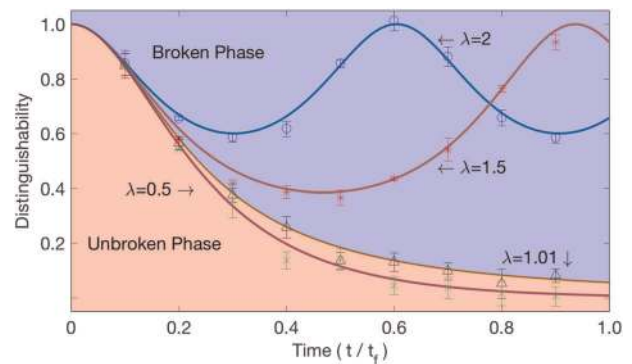

Fig. 3 Experimental results of information flow measured by distinguishability. Four λ values are set in our experiment including three broken anti-$\mathcal{PT}$-symmetric phase and one unbroken point. The solid lines represent theoretical values, and the nine discrete points on each line are experimental results. Theoretical error range of distinguishability are numerically analyzed based on the assumption that the fluctuations of amplitude and phase are within a range of 5%.

broken and information can retrieve from the environment completely. Considering the Breuer-Laine-Piilo (BLP) condition for non-Markovianity[39,53,54], the increase of distinguishability in the broken phase ($\mathrm{d}D(t)/\mathrm{d}t > 0$) implies that there exist memory effects and give rise to a unique non-Markovian process in the anti-$\mathcal{PT}$-symmetric system. The closer parameters get to the exceptional point, the bigger the period gets and the larger the amplitude of information vibration becomes, which means the system undergoes larger fluctuations. However, the distinguishability decays with time and no information recover from the environment in the unbroken anti-$\mathcal{PT}$-symmetric phase. The distinguishability oscillates with period $T = \pi\hbar/(s\sqrt{\lambda^2 - 1})$ and in order to validate our experimental results about change trend, we theoretically analyze the oscillation period and amplitude just as shown in Fig. 4. It can be concluded that the intensity of oscillation is related to the parameter λ and with the
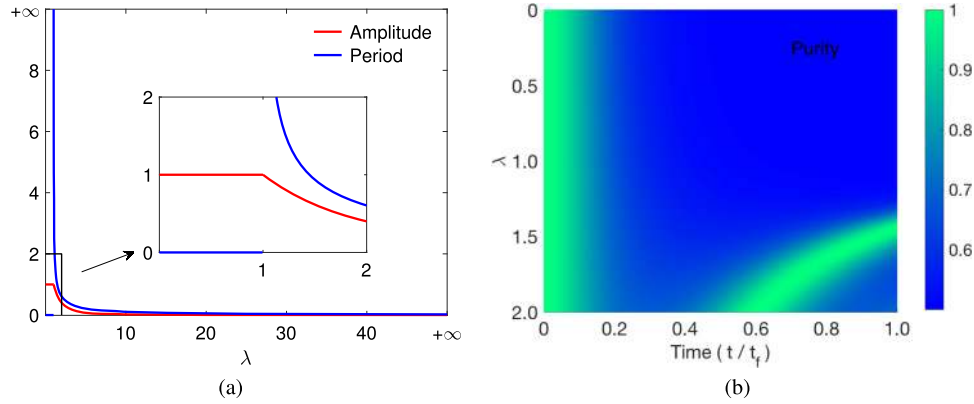
(a)   (b)

Fig. 4 Distinguishability and purity in the anti-$\mathcal{PT}$-symmetric system. a The amplitude and period of distinguishability as functions of λ according the same parameter setup in experiment. The locally enlarged subgraph is the change trend around exceptional point and at the exceptional point $\lambda = 1$ in the inset, there is no information backflow as in the unbroken phase. **b** Purity of quantum state evolving with time under different λ values. When parameters locate in the unbroken anti-$\mathcal{PT}$-symmetric phase ($\lambda < 1$), purity will decay exponentially with time and approach value 0.5, which means a maximum mixed state. The oscillation of purity can be observed in the broken phase.

increasement of λ, the ratio of Hermitian ($\lambda\hat{\sigma}_z$) to non-Hermitian ($i\hat{\sigma}_x$) components in the system Hamiltonian gradually increases, and oscillation of information flow gradually weakens. In the limit case, it reverts to hermitian quantum mechanics, in which the information flow does not oscillate. In the symmetry-unbroken phase, the amplitude keeps value one and the period is zero, which means the system will lose all the information into the environment and information backflow does not occur. Therefore, the behavior of the system can be consistently understood and interpreted, whether it is a Hermitian or an anti-$\mathcal{PT}$-symmetric system. To further determine the evolution characteristics, we theoretically calculated the purity of the quantum state in Fig. 4 and observed similar oscillation and attenuation phenomena just like information flow. This means that the quantum state evolving under the anti-$\mathcal{PT}$-symmetric Hamiltonian will be entangled with the environment so as to a decoherence process, but the process is reversible in the case of broken phase and irreversible in the unbroken phase.

In summary, we propose an algorithm for the simulation of generalized anti-$\mathcal{PT}$-symmetric system and observe an oscillation of information flow in the experiment. We compare the performance when system parameters approach exceptional point and change from anti-$\mathcal{PT}$-symmetric broken phase into unbroken phase. It is found that both the oscillation period and amplitude increase monotonically before the phase transition, whereas no information will be retrieved from the environment any more after passing the critical point, which means that we have also realized a symmetry-breaking process in anti-$\mathcal{PT}$-symmetric system. The monotone correspondence relation in symmetry-broken phase implies that our results could supply a metric method to measure the degree of non-hermiticity ($\propto$ amplitude $\in [0, 1]$) for a quantum system. The change tendency of the information flow obtained in our experiment could supply a consistent understanding method for the Hermitian and anti-$\mathcal{PT}$-symmetric systems. Moreover, we found that there exists an interesting anti-corresponding relation: when $\mathcal{PT}$-symmetry is broken, there is no information flow oscillation, whereas in the broken phase of anti-$\mathcal{PT}$-symmetric system, there is information backflow. This work has important theoretical and experimental implication in the exploration of the interaction between system and the environment and our proposed scheme can be extended to high-dimensional cases and other quantum computing platforms.

METHODS

Experimental setup

In experiments, we use ^{13}C-labeled transcrotonic acid dissolved in d6-acetone as the four-qubit sample. The structure of this molecule is shown in Fig. 5. Notations C1 to C4 denote the four qubits that we can control, and C1 and C2 are chosen as the ancillary qubits, C3 and C4 as the system qubits, respectively. All the ^1H are decoupled throughout the experiment. The experiments were carried out on a Bruker ADVANCE 600 MHz spectrometer at room temperature (298 K). The internal Hamiltonian of the sample under weak coupling approximation is

$$H_{int} = -\sum_{i=1}^{4} \pi\nu_i\sigma_z^i + \sum_{i<j}^{4} \frac{\pi}{2}J_{ij}\sigma_z^i\sigma_z^j, \quad (10)$$

where ν_i is the chemical shift and J_{ij} is the J-coupling strength between the ith and jth nuclei. In Fig. 5, the molecular parameters are listed in the diagonal and off-diagonal elements.

Initialization. The process of quantum computation in liquid nuclear magnetic resonance system starts from a thermal equilibrium state obeying Boltzmann distribution at room temperature T:

$$\rho_{eq} = \frac{e^{-H_{int}/k_B T}}{Tr(e^{-H_{int}/k_B T})}, \quad (11)$$

where k_B is the Boltzmann constant[55]. It is normal that $\|H_{int}/k_B T\|$ is much less than one and $J_{kl} \ll \omega_i$, so that the thermal equilibrium state can be approximated as

$$\rho_{eq} \approx \frac{1}{2^4}\left(I^{\otimes 4} + \sum_i^4 \frac{\hbar w_i \sigma_z^i}{2k_B T}\right), \quad (12)$$

where the notation I is identity matrix and σ_z is a Pauli matrix. To initialize the system, we generally need to drive the quantum system from the highly mixed state ρ_{eq}, which cannot be used as an initial state to the pseudo-pure state in Eq. (8). This is realized via spatial averaging technique[44,45], where all the processes are realized by unitary operations including single-qubit rotations, controlled-NOT gates and gradient fields in the z direction. Full quantum state tomography[48–50] is then performed in order to obtain a quantitative estimation of the quality of our pseudo-pure state. We found that the fidelity between the prepared pseudo-pure state and the target state is over 99% and this state serves as the starting point for subsequent computation tasks.

Readout. The measurement in nuclear magnetic resonance detection is performed on a bulk ensemble of molecules, which means the readout is an ensemble-averaged macroscopic measurement. At the end of the quantum circuit, all experimental data are extracted from the free-induction decay (FID), which is the signal induced by the precessing magnetization of the sample in a surrounding detection coil. FID is recorded as a time-domain signal, which consists of a number of oscillating
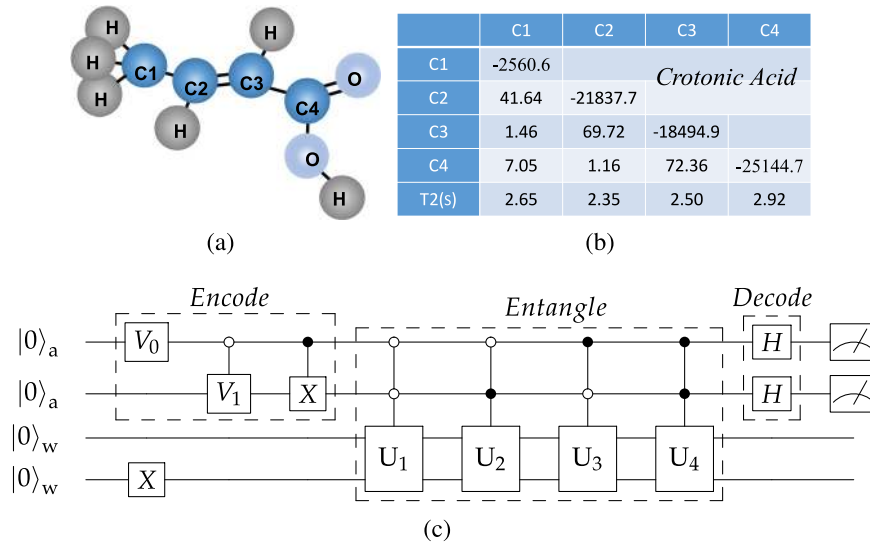
Fig. 5 **Experimental scheme for simulation. a** Molecule structure of ^{13}C-labeled crotonic-acid. C1, C2, C3, and C4 are used as four qubits in the experiment, while all ^1H are decoupled throughout the experiment. **b** Molecule parameters of sample: the chemical shifts and J-couplings (in Hz) are listed by the diagonal and off-diagonal elements, respectively. Transversal relaxation time T2 (in seconds) are also shown at bottom. **c** Quantum circuit used to observe information flow in experiment. The first two qubits are used as ancillary qubits $|00\rangle_a$ and the other qubits are working system $|00\rangle_w$. After a series of unitary quantum gates, we measure the state of the working qubits when the ancillary qubits are $|00\rangle\langle00|$.
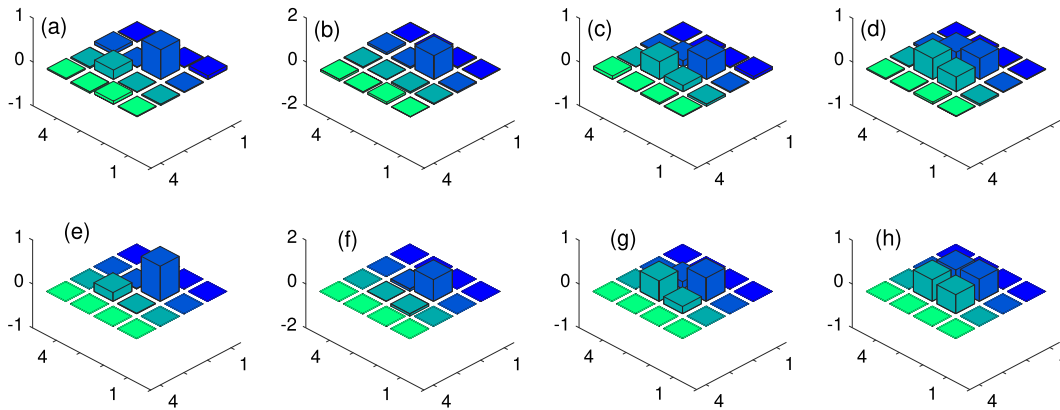
Fig. 6 **Real parts of quantum state of work system at the ninth time points.** Figures in the first row from **a** to **d** represent the real part of the final experimental density matrix ($\lambda_1 \rightarrow \lambda_4$) and the corresponding theoretical values are shown on the following row from **e** to **h**.

waves of different frequencies, amplitudes, and phases. The signal is then subjected to Fourier transformation, and the resulting spectral lines are fitted, yielding a set of measurement data [55]. We obtain the final density matrix by performing quantum state tomography. It is finished by applying 17 readout pulses with a duration of 0.9 ms after the evolution. Then we can reconstruct all the density matrix elements of the final state. We find the subspace where the ancillary qubits are state $|00\rangle\langle00|$ to get the target quantum state of the work system. The real parts of the density matrices of work system for the experimental results at the last time point under different λ values and the corresponding theoretical values are displayed in Fig. 6 to evaluate the performance of our experiment.

Experimental protocol

In experiment, the eigenvalues of the anti-$\mathcal{PT}$-symmetric Hamiltonian H_{APT} in Eq. (7) are $\pm s\sqrt{\lambda^2 - 1}$ and the anti-$\mathcal{PT}$-symmetry will be unbroken if $\lambda < 1$, and the two-order exceptional point is located at $\lambda = 1$. The dynamic evolution under H_{APT} can be realized via our protocol presented above by setting the parameters in Eq. (1) as $\theta = 0$ and $r = \lambda s = \lambda \mu$ appropriately. We fix evolution time $t_f = 1s$ and set $s = 3$ as the energy scale. To reduce the random error caused by the change of environment

in experiment, we extend the controlled gates $U_i = \sigma_i$ to two-qubit Hilbert space $U_i = \sigma_i \otimes \sigma_i$ ($i \in \{0, x, y, z\}$) and add one more rotation σ_x on the second work qubit. Therefore, the quantum systems in two different Hilbert spaces undergo the same dynamic evolution induced by the anti-$\mathcal{PT}$-symmetric Hamiltonian only with different initial state by this experimental setup.

Because the encoding procedure only introduces a constraint on the fist column of the operator, $\sqrt{a_i/a}|i\rangle\langle0|$ ($i = 1, ...d$). To realize it in the circuit-based quantum computer, we decompose it into single-qubit operator V_0 and controlled operators $V_k(k = 1, 2)$ as shown in the dotted box of Fig. 1. According to the parameters of Eq. (4), we can get the explicit forms of the operators:

$$V_0 = \begin{pmatrix} \sqrt{|V'_{11}|^2 + |V'_{21}|^2} & \sqrt{|V'_{31}|^2 + |V'_{41}|^2} \\ \sqrt{|V'_{31}|^2 + |V'_{41}|^2} & -\sqrt{|V'_{11}|^2 + |V'_{21}|^2} \end{pmatrix} = R(\theta_0),$$

$$V_k = \begin{pmatrix} \frac{V'_{2k-1,1}}{\sqrt{|V'_{2k-1,1}|^2 + |V'_{2k,1}|^2}} & \frac{V'_{2k,1}}{\sqrt{|V'_{2k-1,1}|^2 + |V'_{2k,1}|^2}} \\ \frac{V'_{2k,1}}{\sqrt{|V'_{2k-1,1}|^2 + |V'_{2k,1}|^2}} & \frac{-V'_{2k-1,1}}{\sqrt{|V'_{2k-1,1}|^2 + |V'_{2k,1}|^2}} \end{pmatrix} = R(\theta_k),$$

(13)

where the angles in the rotation operators $R(\theta_l) = \begin{pmatrix} \cos\theta_l & \sin\theta_l \\ \sin\theta_l & -\cos\theta_l \end{pmatrix}$, $(l = 0, 1, 2)$ can be determined by

$$\theta_0 = \arccos\sqrt{\frac{w^2\cos^2(wt/2h)+(\mu+s)^2\sin^2(wt/2h)}{w^2+2(\mu+s)^2\sin^2(wt/2h)}},$$

$$\theta_1 = \arccos\frac{w\cos(wt/2h)}{\sqrt{w^2\cos^2(wt/2h)+(\mu+s)^2\sin^2(wt/2h)}}, \quad (14)$$

$$\theta_2 = \arccos\frac{i(s-\mu)}{\sqrt{(\mu-s)^2+4r^2\cos^2\theta}}.$$

Quantum circuit that is used to observe information flow in the experiment is shown in the Fig. 5. Single-qubit operator V_0 and two-qubit operator V_1 are parameter-dependent quantum gates, while the other unitary quantum gates including the controlled-U_i on the working system do not vary with the parameters in the anti-$\mathcal{PT}$-symmetric Hamiltonian. Quantum evolution according to the quantum circuit we constructed are optimized by gradient ascent pulse engineering (GRAPE)[47] with fidelity over 99.5% and the durations of the optimized pulses are within 60 ms in experiment.

DATA AVAILABILITY
The data and the code that support the findings of this study are available from the corresponding author upon reasonable request.

REFERENCES
1. Bender, C. M. & Boettcher, S. Real spectra in non-hermitian hamiltonians having symmetry. *Phys. Rev. Lett.* **80**, 5243 (1998).
2. Konotop, V. V., Yang, J. & Zezyulin, D. A. Nonlinear waves in $\mathcal{PT}$-symmetric systems. *Rev. Mod. Phys.* **88**, 035002 (2016).
3. El-Ganainy, R. et al. Non-hermitian physics and $\mathcal{PT}$ symmetry. *Nat. Phys.* **14**, 11 (2018).
4. Milburn Thomas, J. et al. General description of quasiadiabatic dynamical phenomena near exceptional points. *Phys. Rev. A* **92**, 052124 (2015).
5. Heiss, D. Mathematical physics: circling exceptional points. *Nat. Phys.* **12**, 823 (2016).
6. Bender, C. M., Brody, D. C., Jones, H. F. & Meister, B. K. Faster than hermitian quantum mechanics. *Phys. Rev. Lett.* **98**, 040403 (2007).
7. Zheng, C., Hao, L. & Long, G. L. Observation of a fast evolution in a parity-time-symmetric system. *Philos. Trans. R. Soc. A Math., Phys. Eng. Sci.* **371**, 20120053 (2013).
8. Xiao, L. et al. Observation of topological edge states in parity-time-symmetric quantum walks. *Nat. Phys.* **13**, 1117 (2017).
9. Tang, J.-S. et al. Experimental investigation of the no-signalling principle in parity-time symmetric theory using an open quantum system. *Nat. Photonics* **10**, 642 (2016).
10. Li, J. et al. Observation of parity-time symmetry breaking transitions in a dissipative floquet system of ultracold atoms. *Nat. Commun.* **10**, 855 (2019a).
11. Wu, Y. et al. Observation of parity-time symmetry breaking in a single-spin system. *Science* **364**, 878–880 (2019).
12. Naghiloo, M., Abbasi, M., Joglekar, Y. N. & Murch, K. W. Quantum state tomography across the exceptional point in a single dissipative qubit. *Nat. Phys.* **15**, 1232–1236 (2019).
13. Kawabata, K., Ashida, Y. & Ueda, M. Information retrieval and criticality in parity-time-symmetric systems. *Phys. Rev. Lett.* **119**, 190401 (2017).
14. Lee, Y.-C., Hsieh, M.-H., Flammia, S. T. & Lee, R.-K. Local $\mathcal{PT}$ symmetry violates the no-signaling principle. *Phys. Rev. Lett.* **112**, 130404 (2014a).
15. Chen, S.-L., Chen, G.-Y. & Chen, Y.-N. Increase of entanglement by local $\mathcal{PT}$-symmetric operations. *Phys. Rev. A* **90**, 054301 (2014).
16. Bender, C. M., Brody, D. C. & Jones, H. F. Complex extension of quantum mechanics. *Phys. Rev. Lett.* **89**, 270401 (2002).
17. Bender, C. M., Hook, D. W., Meisinger, P. N. & Wang, Q.-h Complex correspondence principle. *Phys. Rev. Lett.* **104**, 061601 (2010).
18. Ge, L. & Türeci, H. E. Antisymmetric $\mathcal{PT}$-photonic structures with balanced positive-and negative-index materials. *Phys. Rev. A* **88**, 053810 (2013).
19. Yang, F., Liu, Y.-C. & You, L. Anti-$\mathcal{PT}$ symmetry in dissipatively coupled optical systems. *Phys. Rev. A* **96**, 053845 (2017).
20. Li, Q. et al. Experimental simulation of anti-parity-time symmetric Lorentz dynamics. *Optica* **6**, 67–71 (2019b).
21. Konotop, V. V. & Zezyulin, D. A. Odd-time reversal $\mathcal{PT}$ symmetry induced by an anti-$\mathcal{PT}$-symmetric medium. *Phys. Rev. Lett.* **120**, 123902 (2018).
22. Ke, S. et al. Topological bound modes in anti-$\mathcal{PT}$-symmetric optical waveguide arrays. *Opt. express* **27**, 13858–13870 (2019).
23. Zhang, X.-L., Jiang, T., Sun, H.-B. & Chan, C. T. Dynamically encircling an exceptional point in anti-$\mathcal{PT}$-symmetric systems: asymmetric mode switching for symmetry-broken states. *Light Sci. Appl.* **8**, 1–9 (2019).
24. Peng, P. et al. Anti-parity–time symmetry with flying atoms. *Nat. Phys.* **12**, 1139 (2016).
25. Chuang, Y.-L. et al. Realization of simultaneously parity-time-symmetric and parity-time-antisymmetric susceptibilities along the longitudinal direction in atomic systems with all optical controls. *Opt. Express* **26**, 21969–21978 (2018).
26. Wang, X. & Wu, J.-H. et al. Optical $\mathcal{PT}$-symmetry and $\mathcal{PT}$-antisymmetry in coherently driven atomic lattices. *Opt. Express* **24**, 4289–4298 (2016).
27. Choi, Y., Hahn, C., Yoon, J. W. & Song, S. H. Observation of an anti-$\mathcal{PT}$-symmetric exceptional point and energy-difference conserving dynamics in electrical circuit resonators. *Nat. Commun.* **9**, 2182 (2018).
28. Li, Y. et al. Anti-parity-time symmetry in diffusive systems. *Science* **364**, 170–173 (2019).
29. Lee, T. E., Reiter, F. & Moiseyev, N. Entanglement and spin squeezing in non-hermitian phase transitions. *Phys. Rev. Lett.* **113**, 250401 (2014).
30. Couvreur, R., Jacobsen, J. L. & Saleur, H. Entanglement in nonunitary quantum critical spin chains. *Phys. Rev. Lett.* **119**, 040601 (2017).
31. Chakraborty, S. & Chruściński, D. Information flow versus divisibility for qubit evolution. *Phys. Rev. A* **99**, 042105 (2019).
32. Haseli, S. et al. Non-Markovianity through flow of information between a system and an environment. *Phys. Rev. A* **90**, 052118 (2014).
33. Bender, C. M. $\mathcal{PT}$-symmetric quantum state discrimination. *Philos. Trans. R. Soc. A Math. Phys. Eng. Sci.* **371**, 20120160 (2013).
34. Gui-Lu, L. General quantum interference principle and duality computer. *Commun. Theor. Phys.* **45**, 825 (2006).
35. Wiebe, N. & Childs, A. M. Hamiltonian simulation using linear combinations of unitary operations. *Bull. Am. Phys. Soc.* **57**, http://arXiv.org/1202.5822 (2012).
36. Wen, J. et al. Experimental demonstration of a digital quantum simulation of a general $\mathcal{PT}$-symmetric system. *Phys. Rev. A* **99**, 062122 (2019).
37. Bennett, C. H. et al. Purification of noisy entanglement and faithful teleportation via noisy channels. *Phys. Rev. Lett.* **76**, 722 (1996a).
38. Bennett, C. H., Bernstein, H. J., Popescu, S. & Schumacher, B. Concentrating partial entanglement by local operations. *Phys. Rev. A* **53**, 2046 (1996).
39. Breuer, H.-P., Laine, E.-M. & Piilo, J. Measure for the degree of non-Markovian behavior in open systems. *Phys. Rev. Lett.* **103**, 210401 (2009).
40. Brody, D. C. & Graefe, E. M. Mixed-state evolution in the presence of gain and loss. *Phys. Rev. Lett.* **109**, 230405 (2012).
41. Low, G. H. & Chuang, I. L. Hamiltonian simulation by qubitization. *Quantum* **3**, 163 (2019).
42. Low, G. H. & Chuang, I. L. Optimal hamiltonian simulation by quantum signal processing. *Phys. Rev. Lett.* **118**, 010501 (2017).
43. Zheng, C. Duality quantum simulation of a generalized anti-$\mathcal{PT}$-symmetric two-level system. *EPL (Europhys. Lett.)* **126**, 30005 (2019).
44. Cory, D. G., Fahmy, A. F. & Havel, T. F. Ensemble quantum computing by NMR spectroscopy. *Proc. Natl Acad. Sci. USA* **94**, 1634–1639 (1997).
45. Hou, S.-Y., Sheng, Y.-B., Feng, G.-R. & Long, G.-L. Experimental optimal single qubit purification in an NMR quantum information processor. *Sci. Rep.* **4**, 6857 (2014).
46. Fortunato, E. M. et al. Design of strongly modulating pulses to implement precise effective hamiltonians for quantum information processing. *J. Chem. Phys.* **116**, 7599–7606 (2002).
47. Khaneja, N., Reiss, T., Kehlet, C., Schulte-Herbrüggen, T. & Glaser, S. J. Optimal control of coupled spin dynamics: design of NMR pulse sequences by gradient ascent algorithms. *J. Magn. Reson.* **172**, 296–305 (2005).
48. Lee, J.-S. The quantum state tomography on an NMR system. *Phys. Lett. A* **305**, 349–353 (2002).
49. Leskowitz, G. M. & Mueller, L. J. State interrogation in nuclear magnetic resonance quantum-information processing. *Phys. Rev. A* **69**, 052302 (2004).
50. Li, J. et al. Optimal design of measurement settings for quantum-state-tomography experiments. *Phys. Rev. A* **96**, 032307 (2017).
51. Luo, Z. et al. Quantum simulation of the non-fermi-liquid state of Sachdev-Ye-Kitaev model. *npj Quantum Inf.* **5**, 53 (2019).
52. Lu, D. et al. Tomography is necessary for universal entanglement detection with single-copy observables. *Phys. Rev. Lett.* **116**, 230501 (2016).
53. Breuer, H.-P., Laine, E.-M., Piilo, J. & Vacchini, B. Colloquium: non-Markovian dynamics in open quantum systems. *Rev. Mod. Phys.* **88**, 021002 (2016).
54. Rivas, A., Huelga, S. F. & Plenio, M. B. Entanglement and non-Markovianity of quantum evolutions. *Phys. Rev. Lett.* **105**, 050403 (2010).

55. Xin, T. et al. Nmrcloudq: a quantum cloud experience on a nuclear magnetic resonance quantum computer. *Sci. Bull.* **63**, 17–23 (2018).

AUTHOR CONTRIBUTIONS

J.W. proposed the theoretical approach; J.W. and T.X. designed and performed the experimental scheme; T.X. equivalently supervised the project with G.L.; all the authors wrote and modified the paper.

COMPETING INTERESTS

The authors declare no competing interests.

ADDITIONAL INFORMATION

Correspondence and requests for materials should be addressed to T.X. or G.L.

Reprints and permission information is available at http://www.nature.com/reprints

Publisher's note Springer Nature remains neutral with regard to jurisdictional claims in published maps and institutional affiliations.